

A Test of an Upstream Spline Interpolation Technique for the Advective Terms in a Numerical Mesoscale Model

YTZHAQ MAHRER

Department of Soil and Water Science, The Hebrew University of Jerusalem, Rehovot, Israel

ROGER A. PIELKE

Department of Environmental Sciences, University of Virginia, Charlottesville 22903

(Manuscript received 26 October 1977, in final form 13 March 1978)

ABSTRACT

Upstream interpolation with a cubic spline is used to integrate the advective terms in a two-dimensional hydrostatic primitive equation model. The model is applied to study the problems of air flow over a mountain, and sea and land breezes. Results are compared against existing numerical models and against an identical model which uses a simple upstream differencing scheme for the advective terms. It was found that under certain atmospheric conditions, where the atmosphere is being continuously forced, accurate results may be obtained near the surface even with the simple upstream scheme. Also, it is shown that a sophisticated planetary boundary layer parameterization is needed in order to obtain accurate results in both the lower and upper troposphere.

1. Introduction

Upstream interpolation with a cubic spline as a technique to integrate the advective equation is incorporated into the University of Virginia two-dimensional primitive equation model [the last published version is reported in Mahrer and Pielke (1977b)]. This technique was investigated by Purnell (1976) and was shown to be extremely accurate in conserving both phase and amplitude.

Cubic polynomial splines have been used previously for numerical weather forecasting by Price and MacPherson (1973) to fit spatial variations of a dependent variable in a space-centered integration scheme. However, according to Purnell (1976) their method can cause undesirable growth of short-wave noise if used without dissipation for a nonlinear problem. In this paper we followed Purnell's suggestion and applied the scheme using upstream interpolation, and thereby avoid the problems encountered by Price and MacPherson. One of the purposes of this study is to compare the present version of the model with our past version which used the upstream differencing scheme to approximate the advective terms. The upstream technique has been criticized by many investigators because of its inherent computational dissipation. On the other hand, many researchers have used this scheme successfully and their results compare favorably with observations. Examples of such efforts include Neumann and Mahrer (1971) in the study of sea and land breezes

in Israel, Pielke (1974) in his study of the sea breeze over south Florida, Mahrer and Pielke (1976) in the study of the air flow over Barbados, and Colton (1976) in the forecasts of orographic rainfall over the Sierra Nevada in California.

In this paper the model is applied to the study of air flow over an idealized mountain and a sea and land breeze situation. The following specific cases are studied:

- Air flow over 10 m high bell-shaped hill (in order to compare with linear theory);
- Air flow over 1 km high bell-shaped mountain;
- Sea and land breezes along a flat coastline.

2. Basic equations

The basic two-dimensional equations used in this study, which are identical to those used in our earlier studies (Mahrer and Pielke (1975, 1976, 1977a,b), were transformed from a Cartesian coordinate system (x, z^*, t) by the transformation

$$z^* = \xi \frac{z - z_G}{s - z_G}$$

The governing equations of motion, heat, moisture and continuity in the z^* coordinate system are as

follows:

$$\frac{du}{dt} = fv - fV_\theta - \theta \frac{\partial \pi}{\partial x} + g \frac{z^* - \bar{s}}{s} \frac{\partial z_G}{\partial x} - g \frac{z^*}{\bar{s}} \frac{\partial s}{\partial x} + \left(\frac{\bar{s}}{s - z_G} \right)^2 \frac{\partial}{\partial z^*} \left(K_z^m \frac{\partial u}{\partial z^*} \right) + \frac{\partial}{\partial x} \left(K_H \frac{\partial u}{\partial x} \right), \quad (1)$$

$$\frac{dv}{dt} = -fu + fU_\theta + \left(\frac{\bar{s}}{s - z_G} \right)^2 \frac{\partial}{\partial z^*} \left(K_z^m \frac{\partial v}{\partial z^*} \right) + \frac{\partial}{\partial x} \left(K_H \frac{\partial v}{\partial x} \right), \quad (2)$$

$$\frac{d\theta}{dt} = \left(\frac{\bar{s}}{s - z_G} \right)^2 \frac{\partial}{\partial z^*} \left(K_z^\theta \frac{\partial \theta}{\partial z^*} \right) + \frac{\partial}{\partial x} \left(K_H \frac{\partial \theta}{\partial x} \right) + \frac{\partial \theta}{\partial t} \Big|_{\text{Rad}}, \quad (3)$$

$$\frac{dq}{dt} = \left(\frac{\bar{s}}{s - z_G} \right)^2 \frac{\partial}{\partial z^*} \left(K_z^q \frac{\partial q}{\partial z^*} \right) + \frac{\partial}{\partial x} \left(K_H \frac{\partial q}{\partial x} \right), \quad (4)$$

$$\frac{\partial u}{\partial x} + \frac{\partial w^*}{\partial z^*} - \frac{1}{s - z_G} \left(u \frac{\partial z_G}{\partial x} \right) + \frac{1}{s - z_G} \left(\frac{\partial s}{\partial t} + u \frac{\partial s}{\partial x} \right) = 0, \quad (5)$$

$$\frac{\partial \pi}{\partial z^*} = - \frac{s - z_G}{\bar{s}} \frac{g}{\theta}, \quad (6)$$

where

$$\pi = c_p \left(\frac{p}{p_{00}} \right)^{R/c_p}, \quad (7)$$

$$w^* = \frac{\bar{s}}{s - z_G} w - \frac{z^*}{s - z_G} \left(\frac{\partial s}{\partial t} + u \frac{\partial s}{\partial x} \right) + \frac{z^* - \bar{s}}{s - z_G} \left(u \frac{\partial z_G}{\partial x} \right), \quad (8)$$

$$\frac{d}{dt} = \frac{\partial}{\partial t} + u \frac{\partial}{\partial x} + w^* \frac{\partial}{\partial z^*}. \quad (9)$$

The definitions of the symbols are given in the Appendix.

In order to solve the above set of equations an additional equation for s is needed. By integrating (5) from the surface to the top and assuming that $w^* = 0$ on both boundaries we obtain

$$\frac{\partial s}{\partial t} = - \frac{1}{s} \int_0^{\bar{s}} \left\{ \frac{\partial}{\partial x} [u(s - z_G)] \right\} dz^*. \quad (10)$$

In the soil layer we have

$$\frac{\partial T_s}{\partial t} = \frac{\partial}{\partial z} \left(K_s \frac{\partial T_s}{\partial z} \right), \quad (11)$$

where K_s is the soil heat diffusivity.

3. Boundary layer

The surface layer formulation is based on Businger's (1973) equations, while the top of the planetary boundary layer is calculated according to Deardorff's (1974) technique. Vertical turbulent mixing within the planetary boundary layer is simulated using an eddy exchange coefficient profile. The parameterization scheme is described in more detail in Pielke and Mahrer (1975).

4. Surface energy balance and shortwave and longwave radiation

The surface energy balance equation and the short- and long-wave radiation formulation are described in detail in Mahrer and Pielke (1977a,b).

5. Numerical aspects

a. The cubic spline

The advective terms are evaluated by upstream interpolation with a cubic spline technique which has been shown by Purnell (1976) to be extremely accurate in terms of amplitude and phase preservation.

A cubic spline s_D is a function that has a piecewise continuous second derivative and is defined as a cubic polynomial in each grid interval $x_{i-1} \leq x \leq x_i$. By applying the continuity restraint, we obtain (Ahlberg *et al.*, 1967) a system of N simultaneous linear algebraic equations for the slopes of the spline m_i at nodes x_i for $i = 1, \dots, N$.

The equations for a variable grid size are as follows:

$$\lambda_i m_{i-1} + 2m_i + \mu_i m_{i+1} = 3\lambda_i \frac{\phi_i - \phi_{i-1}}{h_i} + 3\mu_i \frac{\phi_{i+1} - \phi_i}{h_i},$$

$$2m_1 + m_2 = 3 \frac{\phi_2 - \phi_1}{h_2},$$

$$m_{N-1} + 2m_N = 3 \frac{\phi_N - \phi_{N-1}}{h_N},$$

where ϕ_i is the dependent variable and

$$h_i = x_i - x_{i-1},$$

$$\lambda_i = \frac{h_{i+1}}{h_i + h_{i+1}}, \quad \mu_i = 1 - \lambda_i,$$

where $i = 1$ and $i = N$ are the boundary points.

In terms of m_i , the cubic spline in the interval

$[x_{i-1}, x_i]$ is written as

$$s_{\Delta}(x) = m_{i-1} \frac{(x_i - x)^2(x - x_{i-1})}{h_i^2} - m_i \frac{(x - x_{i-1})^2(x_i - x)}{h_i^2} \\ + \phi_{i-1} \frac{(x_i - x)^2[2(x - x_{i-1}) + h_i]}{h_i^3} \\ + \phi_i \frac{(x - x_{i-1})^2[2(x_i - x) + h_i]}{h_i^3}. \quad (12)$$

Following Purnell (1976) the integration scheme for the advective terms will be

$$\phi_i^{n+1} = s_{\Delta}^n(x + \alpha \Delta x),$$

where $\alpha = U(\Delta t / \Delta x)$. That is, to evaluate the change of a dependent variable due to advection we go upstream a distance of $U\Delta t$ from the grid point of interest.

Substituting $x_i - \alpha$ for x in (12) we obtain for $U \geq 0$, after some simple algebraic manipulations,

$$\phi_i^{n+1} = \phi_i^n - m_i \alpha + [3(\phi_{i-1} - \phi_i) + 2m_i + m_{i-1}] \alpha^2 \\ - [m_i + m_{i-1} + 2(\phi_{i-1} - \phi_i)] \alpha^3.$$

For $U < 0$ the spline is evaluated between the points i and $i+1$ and we replace x with $x_i + \alpha$ in an equivalent expression to (12), and obtain

$$\phi_i^{n+1} = \phi_i^n + m_i \alpha - [3(\phi_i - \phi_{i+1}) + 2m_i + m_{i+1}] \alpha^2 \\ + [m_i + m_{i+1} + 2(\phi_i - \phi_{i+1})] \alpha^3.$$

In evaluating the splines for the two-dimensional equation we use the splitting method. That is, the splines are evaluated separately for each direction, and applied so that

$$\phi^{n+1*} = T_x(\phi^n), \\ \phi^{n+1} = T_z(\phi^{n+1*}).$$

Here T_x and T_z are the spatial differencing operators for the spline technique in the x and z directions, respectively.

b. Vertical diffusion

The vertical diffusion terms for a variable grid interval are approximated by

$$\frac{\partial}{\partial z} K \frac{\partial \phi}{\partial z} = K_{j+\frac{1}{2}} \left[\frac{\alpha(\phi_{j+1}^n - \phi_j^n) + \beta(\phi_{j+\frac{1}{2}}^{n+1} - \phi_j^{n+1})}{(z_{j+\frac{1}{2}} - z_{j-\frac{1}{2}})(z_{j+1} - z_j)} \right] \\ - K_{j-\frac{1}{2}} \left[\frac{\alpha(\phi_j^n - \phi_{j-1}^n) + \beta(\phi_j^{n+1} - \phi_{j-1}^{n+1})}{(z_{j+\frac{1}{2}} - z_{j-\frac{1}{2}})(z_j - z_{j-1})} \right], \quad (13)$$

where the superscript n refers to the time step, subscript j to the grid point, and α and β are constants ($\alpha + \beta = 1$). This approximation is unconditionally stable if $\beta \geq \frac{1}{2}$.

With $\alpha = \beta = 0.5$, Eq. (13) becomes the commonly used Crank-Nicholson scheme, which, as shown by

Paegle *et al.* (1976), requires a small time step in order to produce accurate results. However, by selecting $\beta = 0.75$ and $\alpha = 0.25$ they obtained almost identical solutions with a time step 30 times larger. In order to verify their result, we reran our one-dimensional model (Pielke and Mahrer, 1975) for the Wangara Day 33 experiment with $\beta = 0.75$, $\alpha = 0.25$ and a time step of 120 s. As seen in Figs. 1a and 1b the predicted vertical profile of the potential temperature using the new form agrees to within 0.1°C with the explicit approximation which used a variable time step as small as 2 s. The semi-implicit form given by (13) executes about 17 times faster than the explicit representation.

c. Grid structure

The staggered horizontal and vertical grid is identical to the one described by Pielke (1974). The model has been run with 30×12 grid points with a constant horizontal grid spacing 7.5 km. The vertical grid spacing is variable with grid points at heights of 0, 5, 15, 100, 300, 700, 1200, 2000, 3000, 4000, 5000 and 6000 m, for the sea and land breeze experiment, and 0, 50, 100, 500, 1000, 2250, 3500, 4750, 6000, 7250, 8500 and 10 000 m for the mountain runs. For several of the mountain experiments eight levels with spacings of 1250 m were added above 10 km. The time step of the integration was 90 s for the sea breeze experiments and 22.5 s for the air flow over mountain experiments. In the soil layer we used 11 levels with a constant grid spacing of 5 cm.

6. Boundary conditions

The boundary conditions at $z^* = 0$ are given by

$$q_G = F_w q_G |_{\text{SATURATED}} + (1 - F_w) q(1), \\ u = v = w^* = 0,$$

while

$$\left. \begin{aligned} u = U_g, \quad v = V_g, \quad w^* = 0 \\ \pi = \pi(\bar{s}) - g(s - \bar{s}) / [\theta(s) + \frac{1}{2} \gamma_{\text{top}}(s - \bar{s})] \\ q(s) = \text{constant} \end{aligned} \right\}$$

on $z^* = s$. The variable F_w is a measure of surface wetness, $q(1)$ is the specific humidity at the first layer, and γ_{top} is the potential temperature lapse rate at the top of the model.

At the lateral boundaries we used a zero gradient boundary condition for the v , u , θ , π , s and q fields, while w was set to zero. We did not experience any problems with these boundary conditions even in the linear mountain experiment (Section 7b) in which no diffusion was included. This is probably due to the strong dissipation of the spline in the short wavelengths $2\Delta x - 3\Delta x$ (see Table 1).

At the initial time the potential temperature and specific humidity were prescribed, while the velocity profile was calculated as reported by Mahrer and

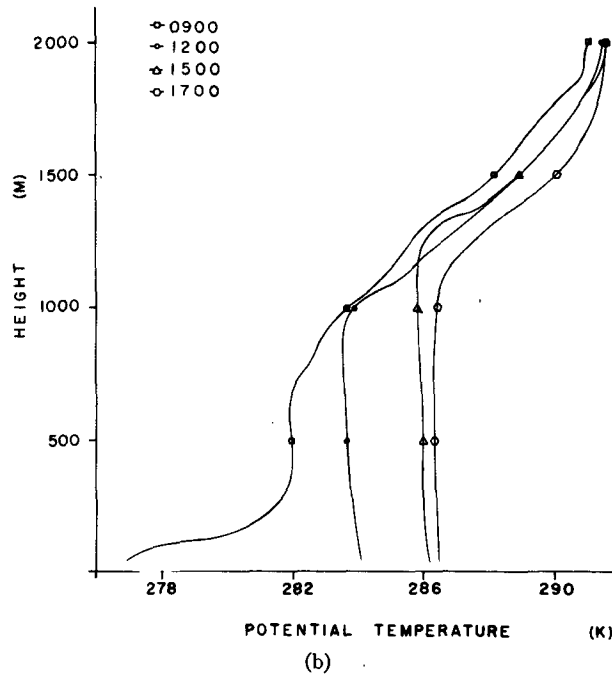
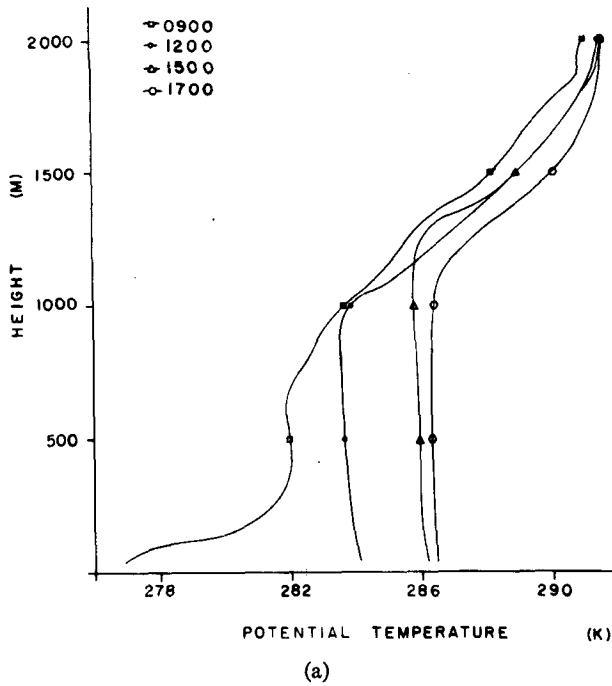


FIG. 1. Vertical profiles of the potential temperature for Wangara Day 33 with (a) the implicit scheme ($\beta=0.75$) and (b) the explicit scheme ($\beta=0$).

Pielke (1976). When topography was present, the equations are initially in approximate computational balance as discussed in Mahrer and Pielke (1977b, p. 1154).

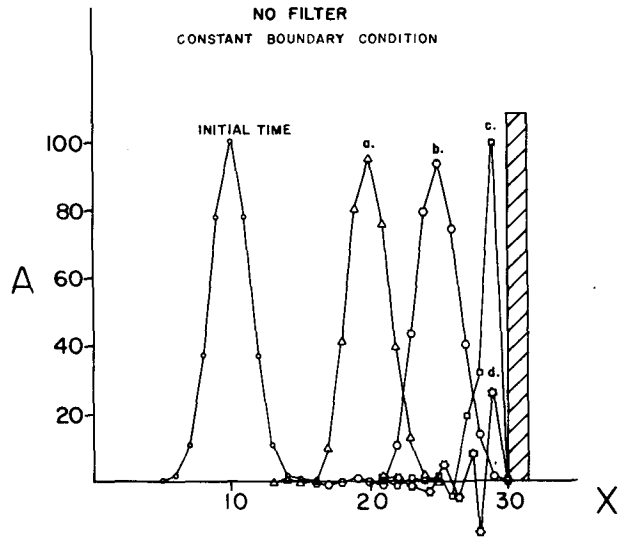


FIG. 2. The initial Gauss function, and its shape and position after it was advected 10 and 15 grid points, and just before and after it reached the boundary for the constant boundary condition.

7. Results

The performance of the cubic spline interpolation method has been tested several ways in our model. The first method involves integrating the one-dimensional linear advection equation, which is given by

$$\frac{\partial \phi}{\partial t} + U_0 \frac{\partial \phi}{\partial x} = 0.$$

Using the spline technique, a Gaussian function of the form

$$\phi = 100 \exp[-0.25(x-x_0)^2]$$

centered at $x_0=10$ in a 30 grid point mesh is advected toward a boundary with (i) a constant boundary condition and, (ii) a gradient boundary condition. The

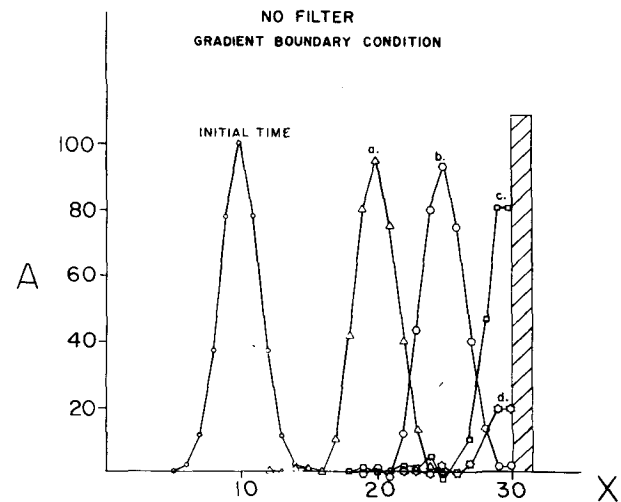


FIG. 3. As in Fig. 2 but for the zero gradient boundary condition.

TABLE 2. Phase for the spline technique (expressed as the ratios between the numerical and correct phases). Table courtesy of Dr. J. Klemp, of NCAR.

Wavelength	Courant number										
	0.0	0.1	0.2	0.3	0.4	0.5	0.6	0.7	0.8	0.9	1.0
2Δx	0	0	0	0	0	1.000	0	0	0	0	0
3Δx	0.810	0.822	0.854	0.901	0.953	1.000	1.031	1.043	-0.802	-0.614	-0.429
4Δx	0.955	0.958	0.967	0.979	0.990	1.000	1.007	1.009	1.008	1.005	1.000
5Δx	0.983	0.985	0.988	0.992	0.996	1.000	1.002	1.003	1.003	1.002	1.000
6Δx	0.993	0.993	0.995	0.997	0.999	1.000	1.001	1.001	1.001	1.001	1.000
8Δx	0.998	0.998	0.998	0.999	0.999	1.000	1.000	1.000	1.000	1.000	1.000
10Δx	0.999	0.999	0.999	1.000	1.000	1.000	1.000	1.000	1.000	1.000	1.000

Klemp and Lilly (1978). As suggested by Klemp and Lilly (1978), eight vertical levels were added at the top of the model, in which the horizontal diffusivity increases with height, in order to absorb reflections from the top. The form of the horizontal smoothing in the absorbing layer is

$$\bar{\phi}_i = (1-b)\phi_i + \frac{1}{2}b(\phi_{i+1} + \phi_{i-1}),$$

where b increases linearly from zero at the bottom of the absorbing layer (z_b) to 0.5 at the top of this layer (z_r); b is thus given as

$$b = 0.5 \frac{z^* - z_b}{z_r - z_b}.$$

The maximum value of b with $\Delta t = 22.5$ and $\Delta x = 7.5$ km is equivalent to a horizontal diffusion coefficient with a value of $K = 6.2 \times 10^5 \text{ m}^2 \text{ s}^{-1}$ and for an $8\Delta x$ wave corresponds to Klemp and Lilly's nondimensional $V (=kv_T/\bar{u})$ of 3.3. We apply the smoother every time step on the u and θ fields.

In the following experiment, which is equivalent to the experiment presented by Klemp and Lilly, we study the air flow over a 10 m bell-shaped mountain. The atmosphere is initially isothermal and has a horizontal wind speed of 20 m s^{-1} . The surface layer has been eliminated and a free slip bottom boundary was applied. Fig. 5 shows the potential temperature field (perturbations have been amplified by a factor of 50 for visualization purposes) after 12 h which corresponds to a dimensionless time of 28.8. Klemp and Lilly (1978) have shown that this time is sufficient to obtain a steady-state solution. The good agreement between the analytic and the numerical solution [both Klemp and Lilly's (Fig. 7 of their paper) and ours] is an encouraging validation of the accuracy of the model.

Fig. 6 shows the vertical profile of the horizontally integrated momentum flux

$$M = \int_{-145 \text{ km}}^{145 \text{ km}} \rho u' w' dx$$

in an $x-z$ coordinate system when the upstream and spline techniques were each used to perform this experi-

ment. With the spline scheme the momentum flux is almost constant within the inviscid layer, as obtained by Klemp and Lilly (1978), while with upstream the momentum flux decreases rapidly with height. However, at the 1 km level the results are very close. This suggests that, when only the lower level circulation is of interest and reflection from the tropopause or other layers in the atmosphere is minimal, the upstream approximation of the advective terms may be an economical way to dissipate upward propagating energy without resorting to a dissipation layer at the top of the model.

b. Air flow over a mountain

To test the mesoscale model for large-amplitude cases where nonlinear terms have a significant effect, we reproduced Klemp and Lilly's (1978, p. 93) experiment with a 1 km bell-shaped mountain. The atmosphere consists of a uniform troposphere extending up to 10 km in which the lapse rate is a constant -6°C km^{-1} and an isothermal stratosphere above. The horizontal wind is initially set at 20 m s^{-1} , with a free slip bottom boundary. A constant horizontal eddy diffusion of

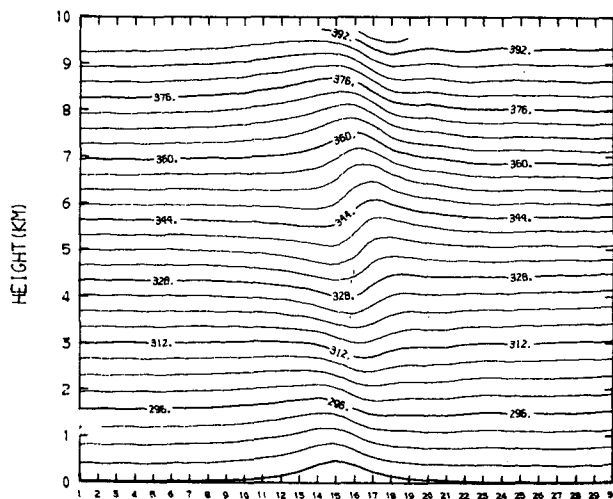


FIG. 5. Potential temperature field (perturbations have been amplified by a factor of 50) after 12 h for the 10 m mountains. Contour interval is 4 K. The geostrophic wind is 20 m s^{-1} from 270° .

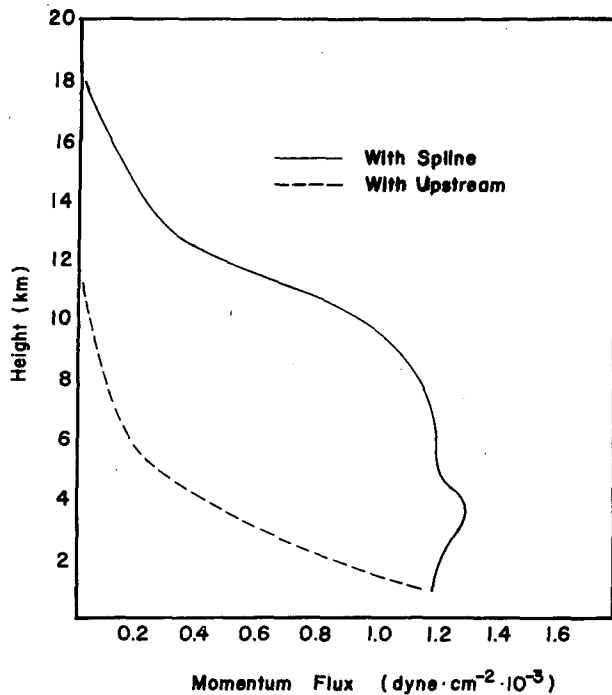


FIG. 6. Vertical profile of the horizontally integrated momentum flux.

$K_H = 1 \times 10^4 \text{ m}^2 \text{ s}^{-1}$ is applied to the u field in order to maintain nonlinear stability. Figs. 7a and 7b show the u component and potential temperature fields after 12 h of integration (only the lower 10 km are shown). The well-known structure of a strong mountain wave, similar to Klemp and Lilly's 1978 result (Fig. 10 in their paper), is reproduced. The results of this experiment show that the model is capable of simulating mountain waves when an absorbing layer is included. Figs. 8a and 8b show the u component and potential temperature fields for the same experiment but with the upstream differencing scheme for the advective terms, and without explicit diffusion in the upper absorbing layer. As seen from the figures the results are very similar in the first 5 km. For example, the maximum horizontal wind at a height of 2.5 km is 29.6 m s⁻¹ with spline, while with upstream it is 27.3 m s⁻¹. Above that level the solutions diverge from one another.

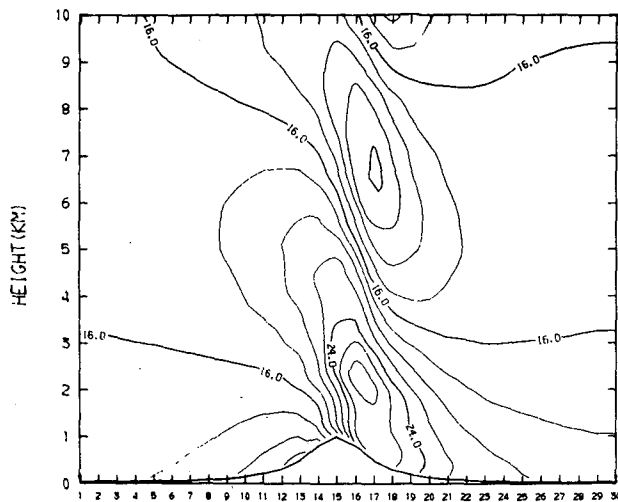


FIG. 7a. The east-west component of the wind after 12 h for the 1 km mountain (with upstream spline interpolation of advection terms). Contour interval is 2 m s⁻¹.

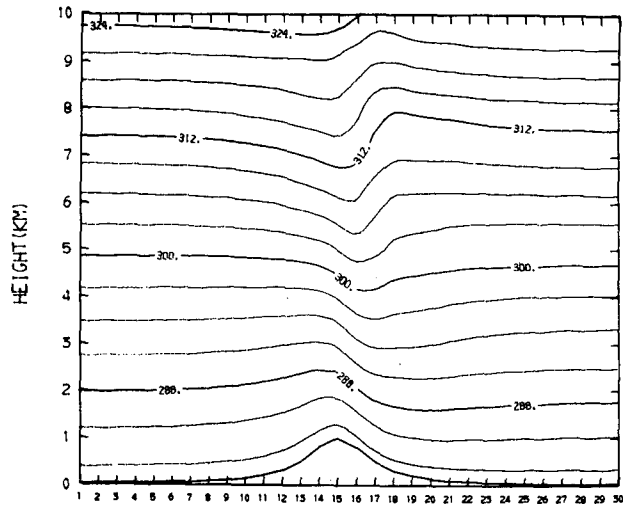


FIG. 7b. The potential temperature after 12 h for the 1 km mountain (with spline). Contour interval is 3 K. The geostrophic wind is 20 m s⁻¹ from 270°.

ture fields for the same experiment but with the upstream differencing scheme for the advective terms, and without explicit diffusion in the upper absorbing layer. As seen from the figures the results are very similar in the first 5 km. For example, the maximum horizontal wind at a height of 2.5 km is 29.6 m s⁻¹ with spline, while with upstream it is 27.3 m s⁻¹. Above that level the solutions diverge from one another.

c. The effect of the surface boundary layer

The following experiment is identical in all respects to the first experiment of the previous section except that the free slip surface boundary condition is replaced by the boundary layer parameterization technique mentioned in Section 3. The u component of velocity and the potential temperature fields are shown in Figs. 9a and 9b. Comparing these figures to Figs. 7a and 7b shows that the planetary boundary layer has a significant influence on the wind and temperature fields even at higher elevations. As expected, the surface winds are much weaker in this case due to friction. For example, the 50 and 100 m winds are reduced by up to 10 m s⁻¹. At higher levels the winds differ by about 1–4 m s⁻¹, with the upper level minimum being at a height of over 9 km instead of 7 km as in Fig. 7a. This suggests that in order to simulate air flow over mountains correctly a realistic planetary boundary layer is necessary. Attempts to simulate real data cases without such a layer will lead to significant errors.

The effect of omitting the absorbing layer and increasing the horizontal eddy diffusion in the entire domain (to $K = 5 \times 10^5 \text{ m}^2 \text{ s}^{-1}$), and retaining the planetary boundary layer is illustrated in Figs. 10a and 10b. In this case the solution near the ground is similar to that in Figs. 9a and 9b, although large differences are apparent higher up.

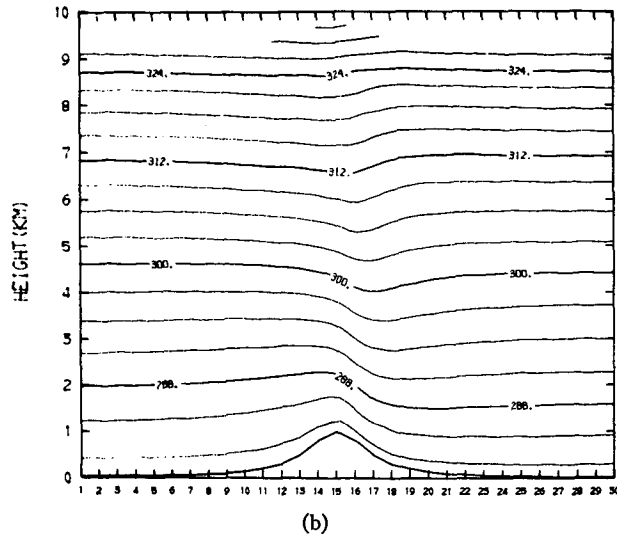
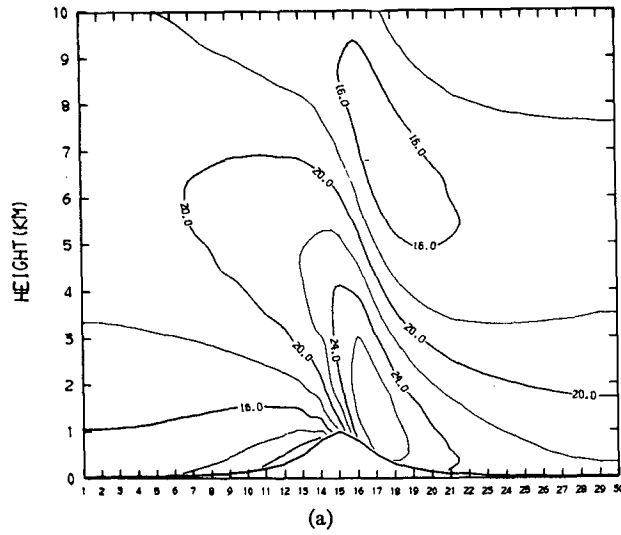


FIG. 8. As in Fig. 7 except with upstream differencing of the advection terms.

The results of these experiments suggest that under many atmospheric conditions accurate results may be obtained near the surface with a damping scheme (like upstream), without the use of an absorbing layer when the solution is being continuously forced. At higher levels, however, a damping layer is required in order to obtain accurate results. Such a layer although necessary under certain atmospheric situations is not economical in three-dimensional models where one is limited by computer storage and execution time. Therefore, the decision to include a damping layer in physically realistic simulations depends on the dominant atmospheric response as well as the levels of interest in the atmosphere. A simulation of the upper tropospheric flow field over high mountains in strong synoptic flow, for example, requires an upper absorbing layer and a computational scheme such as the interpolated cubic

spline. On the other hand, if the interest is in the lowest levels of the troposphere, our results suggest such a layer can be neglected, and the computational scheme need not be so precise.

d. Sea breeze experiment

The upstream differencing scheme is widely used for simulating the sea and land breeze phenomena (e.g., Estoque, 1961; Neumann and Mahrer, 1973, 1974; Pielke, 1974; Mahrer and Pielke, 1977b).

On the other hand, many investigators (e.g., Physick, 1976; Pearson, 1974), use non-dissipative schemes which have been thought to be more accurate for this problem. These schemes, however, are more difficult to implement and somewhat more expensive to use.

In the next set of experiments we will show that for sea breeze problems over flat terrain in which the fields change slowly with time relative to the time step, forward upstream differencing is a satisfactory solution

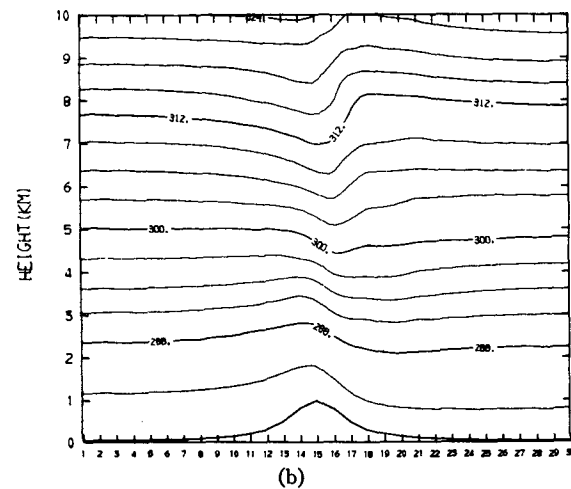
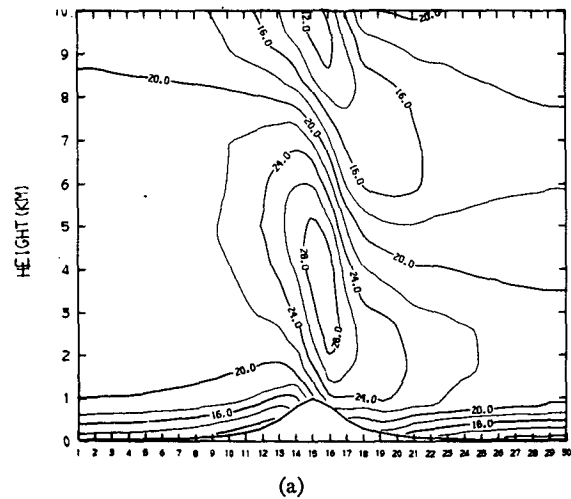
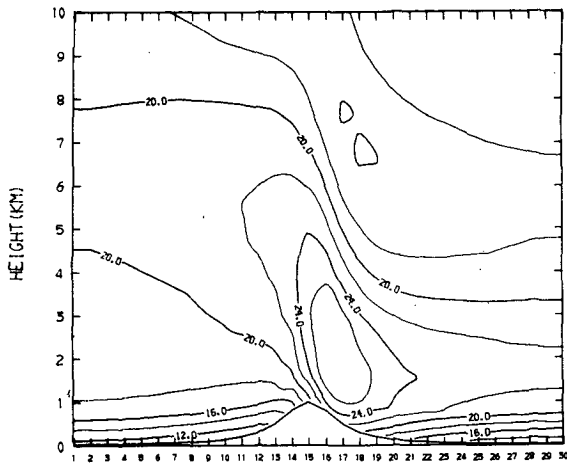
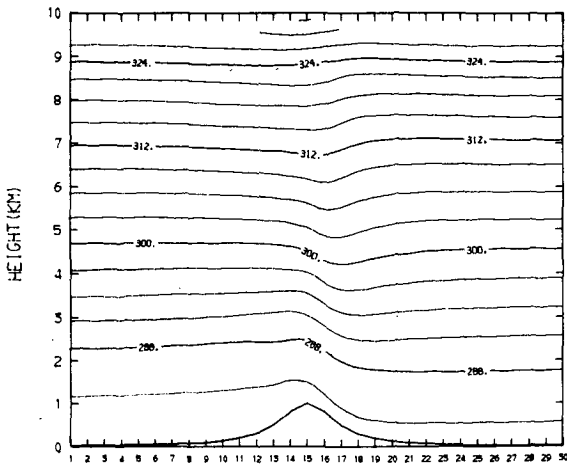


FIG. 9. As in Fig. 7 except when the planetary boundary layer parameterization is included.



(a)



(b)

FIG. 10. As in Fig. 9 but without an absorbing layer and with increased explicit diffusion.

technique. For problems of this sort, the more sophisticated difference schemes add little information. To show this we have performed two identical experiments one with upstream and the other with the interpolated cubic spline technique. In these experiments we initially set the top of the model at a height of 6 km, and prescribed a uniform atmosphere with a lapse rate of $-6.5^{\circ}\text{C km}^{-1}$. The horizontal wind above the planetary

TABLE 3. The remaining amplitude of a wave of 2, 4, 6, 8 and $10\Delta x$ after one application of (14) for values of δ from 0.01 to 1.0

Wavelength	δ				
	0.01	0.05	0.1	0.25	1
$2\Delta x$	0.0	0.0	0.0	0.0	0.0
$4\Delta x$	0.9901	0.9524	0.9091	0.8000	0.500
$6\Delta x$	0.9967	0.9836	0.9677	0.9231	0.7500
$8\Delta x$	0.9983	0.9915	0.9831	0.9589	0.8536
$10\Delta x$	0.9989	0.9947	0.9896	0.9743	0.9045

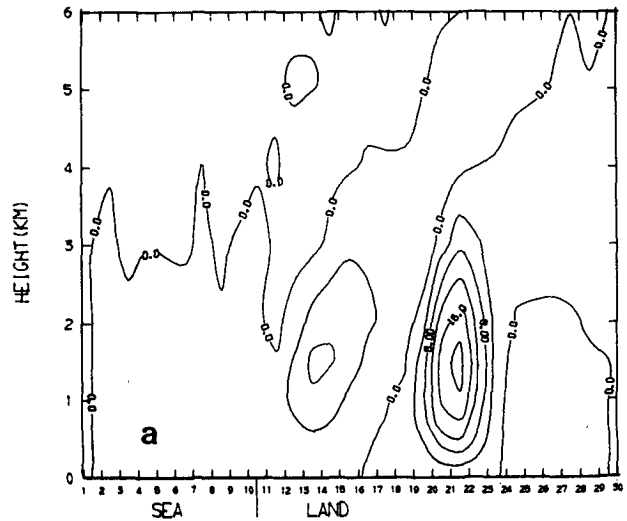
boundary layer was initially set at 1.0 m s^{-1} . To control aliasing we adopted a very selective low-pass filter rather than use a horizontal exchange coefficient formulation. The filter was suggested by Paul Long (personal communication), and is of the form

$$(1-\delta)\bar{\phi}_{i+1}+2(1+\delta)\bar{\phi}_i+(1-\delta)\bar{\phi}_{i-1}=\phi_{i+1}+\phi_{i-1}+2\phi_i,$$

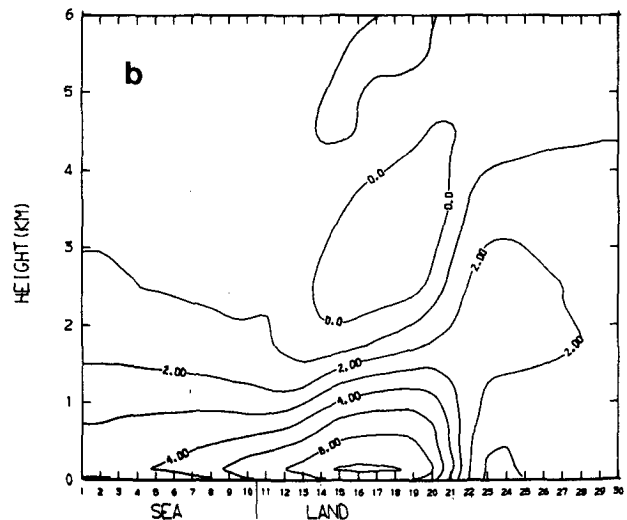
where ϕ is the field to be smoothed and $\bar{\phi}$ the smoothed field. This filter completely eliminates the $2\Delta x$ waves with each application, while its smoothing effect on the other wavelengths is a function of δ . The smoothed field can be related to the original field by

$$\bar{\phi}=\phi\frac{1}{1+\delta\tan^2(\lambda/2)}, \tag{14}$$

where λ is the wavenumber.



TIME = 16.0 HOURS



TIME = 16.0 HOURS

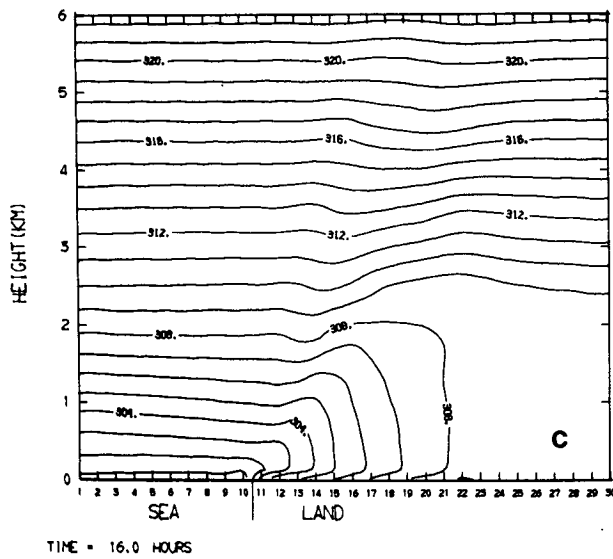
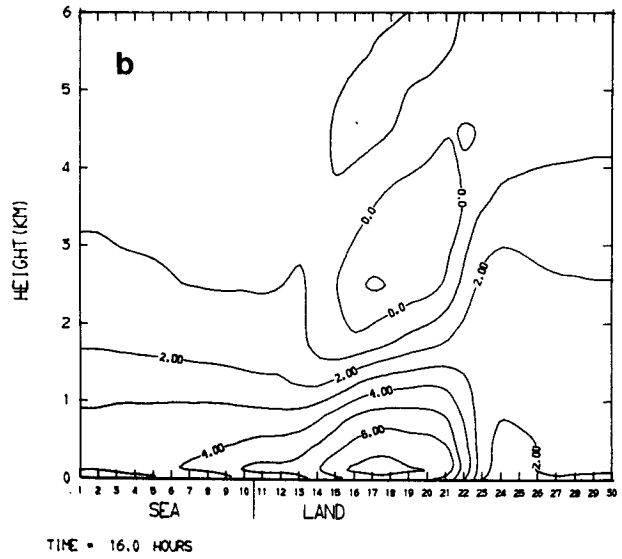


FIG. 11. Vertical velocity (a) (contour interval 4 cm s^{-1}) horizontal velocity (b) (contour interval 1 m s^{-1}) and potential temperature (c) (contour interval 1 K) at 1600 LST with upstream differencing of advection terms. Geostrophic wind of 1 m s^{-1} from 270° .



The response function for one application of Long's filter is given in Table 3. For $\delta \leq 0.1$ there is little damping of waves larger than six grid intervals, while for $\delta = 1$ this filter is equivalent to a 1-2-1 smoother.

The resultant potential temperature, u component of the velocity and vertical velocity fields for the upstream and cubic spline at 1600 LST are shown in Figs. 11 and 12, respectively. As illustrated in the figures the results are almost identical with slightly smoothed fields in the upstream case.

Since upstream differencing introduces a computational diffusion coefficient proportional to the velocity

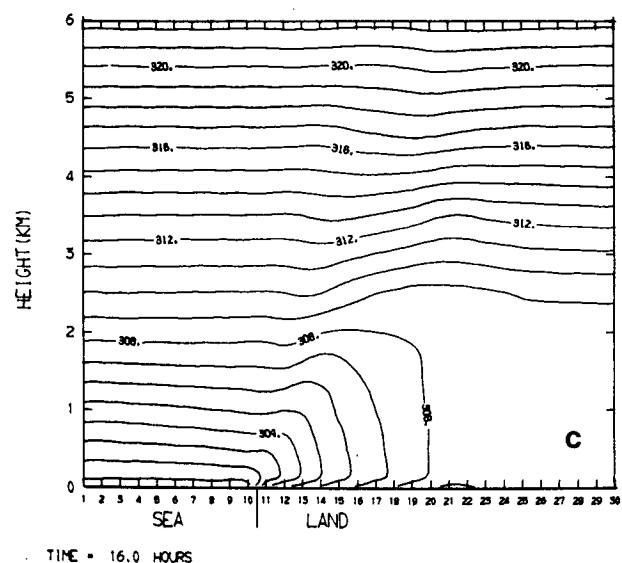
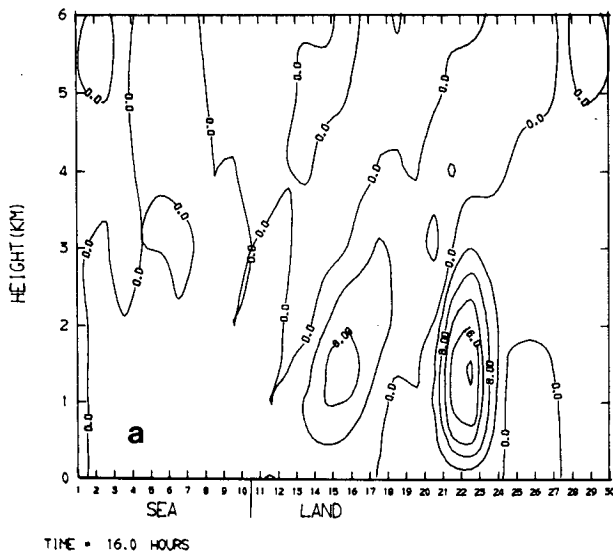


FIG. 12. As in Fig. 11 except with upstream spline interpolation of the advection terms.



and approximately equal to

$$v = \frac{1}{2}u\Delta x(1 - u\Delta t/\Delta x),$$

we reran the above experiment with an initial horizontal wind of 7.5 m s^{-1} . As seen from Figs. 13 and 14, which are for upstream and spline, respectively, the results are almost identical despite the stronger large scale flow. Therefore, both the upstream differencing approximation and the interpolated spline technique are well-suited for use in sea breeze simulations.

These experiments, primarily performed to compare the upstream method with the interpolated spline, also permit us to make some comments relative to the difference in the intensity of the sea breeze convergence with the light (1 m s^{-1}) and the strong (7.5 m s^{-1})

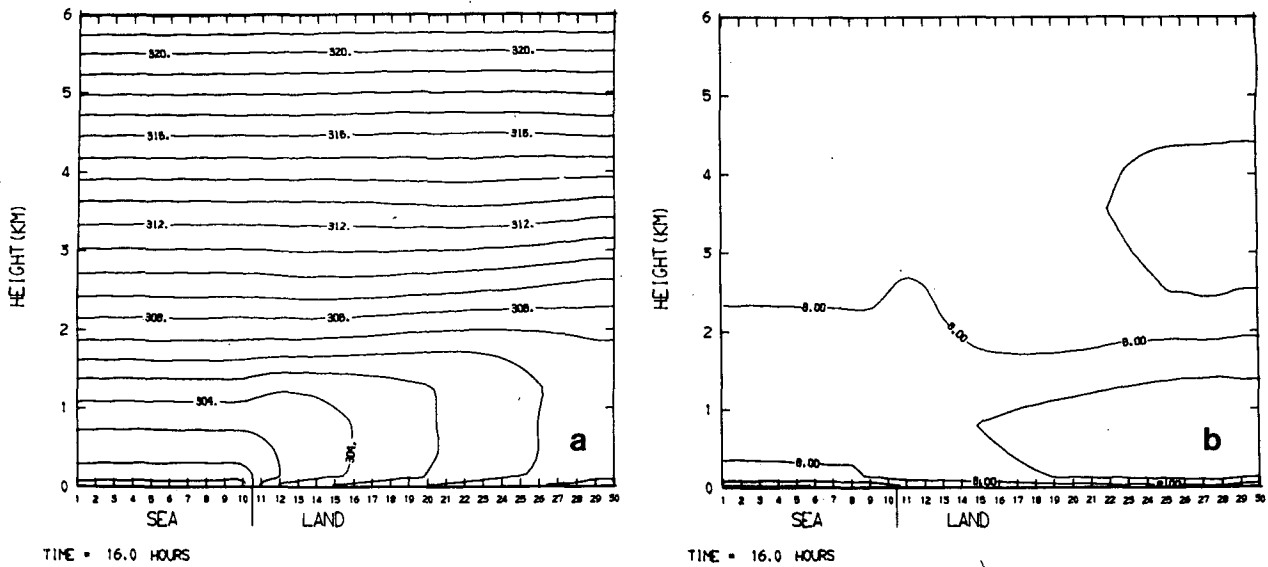


FIG. 13. Potential temperature (a) (contour interval 1 K) and horizontal velocity (b) (contour interval 1 m s⁻¹) at 1600 LST with upstream differencing of the advection terms. Geostrophic wind of 7.5 m s⁻¹ from 270°.

large-scale winds.¹ With the light wind, the sharp temperature contrast between the land and water causes the development of a strong horizontal pressure gradient which results in a tight and well-defined sea breeze circulation, as it moves slowly inland. The stronger large-scale wind, on the other hand, prevents the development of such an intense pressure gradient, since the rapid inland movement of the convergence zone, along with the warming of the marine air as it moves over land, prevents the development of a well-defined temperature maximum at low levels. The

preference for stronger low-level convergence with light synoptic winds may help explain the higher rainfall totals observed over south Florida during the summer, when the sea breeze is generated in a light synoptic flow regime (J. Simpson, University of Virginia, and W. Woodley, NOAA, Boulder, personal communication).

8. Conclusions

It is shown in this study that the model, when used with the cubic spline technique and with an absorbing layer as suggested by Klemp and Lilly (1978), correctly predicts mountain waves at all levels. As shown by

¹ Contrast the horizontal temperature gradient and vertical motion fields between Figs. 12 and 14.

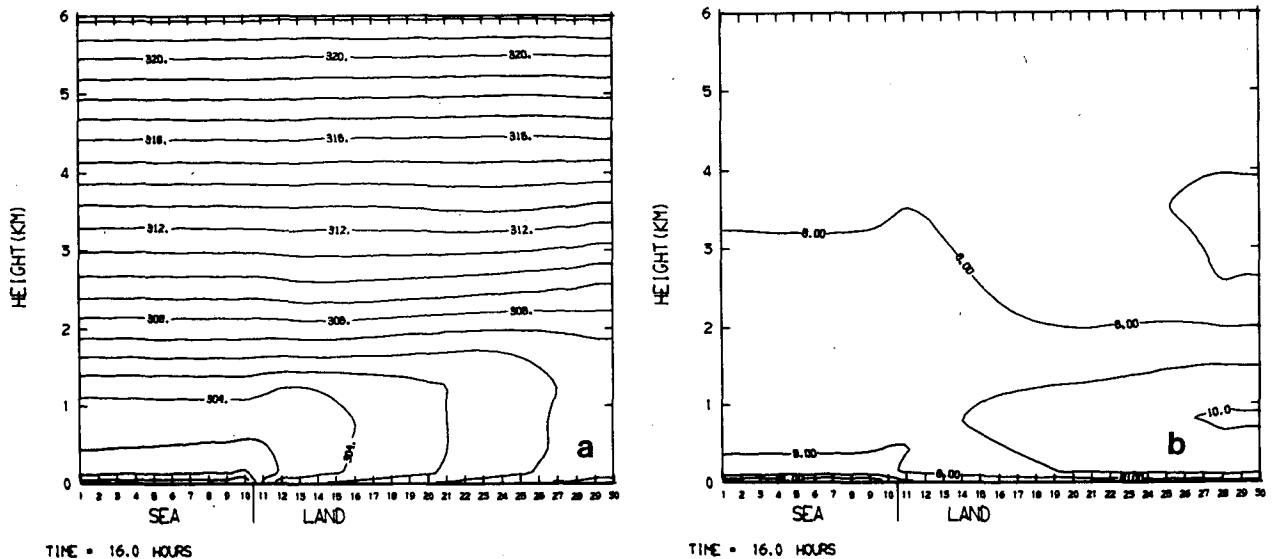


FIG. 14. As in Fig. 13 except with upstream spline interpolation of the advection terms.

Klemp and Lilly (1975), based on linear theory, large-amplitude responses can occur at low levels because of the partial downward reflection of mountain-induced upward propagating energy. These reflections are a result of variations in wind and temperature up to the tropopause level. Their analyses suggest that the optimal response occurs when the vertical phase shift of the wave in the troposphere is about one-half wavelength and when a low-level stable layer exists. When the atmosphere deviates appreciably from these optimal conditions, however, the downward reflection of energy becomes relatively unimportant due to the destructive reinforcement of the wave modes and to turbulent dissipation of shorter wavelength features. For these latter cases, which are by far the more common, accurate results may be obtained near the surface with a dissipative computational scheme or with a conservative scheme with explicit horizontal diffusion. This is an encouraging result when one is interested in experimenting with three-dimensional mesoscale numerical models where the interest is in the flow in the lowest few kilometers.

Our experiments also show that the incorporation of a realistic planetary boundary layer has a significant influence on the wind and temperature fields even at high altitudes, as well as near the ground. Any attempt to simulate real data cases, therefore, without a realistic boundary layer will lead to significant errors.

Simulations of the sea breeze with the upstream and the interpolated spline approximation to the advective terms showed little differences at any level for either the light or strong synoptic flows. Nonetheless, because of the superior accuracy of the spline technique and the need to simulate a wide range of mesoscale circulations, we have adopted the scheme into our three-dimensional version of the model. We plan to run the two-dimensional version of the model with and without the absorbing layer for particular problems in order to see if such a level is needed in the more costly three-dimensional simulations. Linear theory will also provide us guidance in this regard.

Acknowledgments. The authors wish to thank Joe Klemp, Joanne Simpson and William Woodley for their useful comments. An exchange of correspondences with Joe Klemp and Douglas K. Lilly provided the initial impetus for this study and we acknowledge and appreciate their interest and suggestions. James H. S. Bradley, Paul Long and Wilson A. Shaffer are thanked for their advice concerning optimal solution techniques for the prognostic equations in the model. Their suggestions have helped guide our search for better methods of solution. Donna Hensley performed the difficult task of typing and editing the manuscript. This work was supported by National Science Foundation under Grant ATM76-22277. Acknowledgment is made to the National Center for Atmospheric Research, which is

sponsored by the National Science Foundation, for the computer time used in this research.

APPENDIX

List of Symbols

c_p	specific heat at constant pressure
f	Coriolis parameter
F_w	ground moisture measure
g	acceleration of gravity
K_H	horizontal exchange coefficient
K_s	soil heat diffusivity
K_z^m, K_z^0, K_z^q	vertical exchange coefficient of momentum, heat and moisture
p	pressure
p_{00}	reference pressure
q	specific humidity
q_G	surface specific humidity
R	gas constant for dry air
\bar{s}	initial height of the material surface
s	material surface top of the model
s_Δ	cubic spline over a grid interval
T	temperature
u, v, w	east-west, north-south and vertical wind component
U_g, V_g	east-west and north-south geostrophic wind
w^*	vertical (z^*) component of velocity
x, y, z	Cartesian coordinates
z^*	vertical terrain following coordinate
z_G	ground elevation
δ	parameter used in Long's filter [Eq. (14)]
π	Exner's function [= $c_p(p/p_{00})^{R/c_p}$]
θ	potential temperature
γ_{top}	potential temperature lapse rate at the top of the model

REFERENCES

- Ahlberg, J. H., E. N. Nilson and J. L. Walsh, 1967: *The Theory of Splines and their Applications*. Academic Press (see pp. 9-15).
- Businger, J. A., 1973: Turbulent transfer in the atmosphere surface layer. *Workshop in Micrometeorology*, Amer. Meteor. Soc., Chap. 2.
- Colton, D. E., 1976: Numerical simulation of the orographically induced precipitation distribution for use in hydrologic analysis. *J. Appl. Meteor.*, **15**, 1241-1251.
- Crowley, W. P., 1968: Numerical advection experiments. *Mon. Wea. Rev.*, **96**, 1-11.
- Deardorff, J., 1974: Three dimensional numerical study of the height and mean structure of a heated planetary boundary layer. *Bound.-layer Meteor.*, **7**, 81-106.
- Estoque, M. A., 1961: A theoretical investigation of the sea breeze. *Quart. J. Roy. Meteor. Soc.*, **87**, 136-146.
- Klemp, J. B., and D. K. Lilly, 1975: The dynamics of wave-induced downslope winds. *J. Atmos. Sci.*, **32**, 320-339.
- , and —, 1978: Nonlinear numerical simulation of hydrostatic mountain waves. *J. Atmos. Sci.*, **35**, 78-107.
- Mahrer, Y., and R. A. Pielke, 1975: A numerical study of the air flow over mountains using the two-dimensional version of the University of Virginia mesoscale model. *J. Atmos. Sci.*, **32**, 2144-2155.

- , and —, 1976: Numerical simulation of the air flow over Barbados. *Mon. Wea. Rev.*, **104**, 1392–1402.
- , and —, 1977a: A numerical study of the air flow over irregular terrain. *Beil. Phys. Atmos.*, **50**, 98–113.
- , and —, 1977b: The effects of topography on the sea and land breezes in a two dimensional numerical model. *Mon. Wea. Rev.*, **105**, 1151–1162.
- Neumann, J., and Y. Mahrer, 1971: A theoretical study of the land and sea breeze circulation. *J. Atmos. Sci.*, **28**, 532–542.
- , and —, 1974: A theoretical study of the sea and land breezes of circular islands. *J. Atmos. Sci.*, **31**, 2027–2039.
- Orszag, S. A., 1971: Numerical simulation of incompressible flows within simple boundaries: Accuracy. *J. Fluid Mech.*, **49**, 76–112.
- Paegle, J., W. G. Zdunkowski and R. M. Welch, 1976: Implicit differencing of predictive equation of the boundary layer. *Mon. Wea. Rev.*, **104**, 1321–1324.
- Pearson, R. A., 1974: Consistent boundary conditions for numerical model of systems that admit dispersive waves. *J. Atmos. Sci.*, **31**, 1481–1489.
- Physick, W., 1976: A numerical model of the sea-breeze phenomenon over a lake or gulf. *J. Atmos. Sci.*, **33**, 2107–2135.
- Pielke, R. A., 1974: A three dimensional numerical model of the sea breeze over south Florida. *Mon. Wea. Rev.*, **102**, 115–139.
- , and Y. Mahrer, 1975: Technique to represent the heated-planetary boundary layer in mesoscale models with coarse vertical resolution. *J. Atmos. Sci.*, **32**, 2288–2308.
- Price, G. V. and A. K. MacPherson, 1973: A numerical weather forecasting method using cubic splines on a variable mesh. *J. Appl. Meteor.*, **12**, 1102–1113.
- Purnell, D. K., 1976: Solution of the advective equation by upstream interpolation with a cubic spline. *Mon. Wea. Rev.*, **104**, 42–48.